CLM-P 407

NEUTRAL INJECTION HEATING OF A TOKAMAK PLASMA - THEORY AND EXPERIMENT

J.G. CORDEY, E.P. GORBUNOV[≠], J. HUGILL, J.W.M. PAUL, J. SHEFFIELD,

E. SPETH[+], P.E. STOTT, V.I. TERESHIN[*]

Euratom-UKAEA Association for Fusion Research,
Culham Laboratory, Abingdon, Oxon, OX14 3DB, UK

ABSTRACT

A powerful beam of neutral hydrogen is injected tangentially into the plasma produced in the Cleo-Tokamak apparatus. The effect on the macroscopic parameters of the plasma and on the equilibrium are found to be small. The energy spectrum of the resulting fast ions contained in the plasma is deduced from measurements of tangentially emitted charge exchange neutrals. The results for injection parallel and anti-parallel to the plasma current are compared with a classical theoretical model, and good agreement is obtained. Measurements of the perpendicular energy spectrum of 'plasma ions' show that the bulk of the ions are heated by about 10%, and that the low energy ion distribution has a 'tail', which is consistent with the spectrum of decelerated injected ions.

≠ Attached from Kurchatov Institute of Atomic Energy, Moscow D-182, U.S S.R.

\+ Attached from Max-Planck I.P.P., 8046 Garching, W. Germany.

* Attached from Physicotechnical Institute, Academy of Sciences of the Ukrainian SSR, Kharkov, U.S.S.R.

(Submitted for publication in Nuclear Fusion)

November 1974

KS

C O N T E N T S

1. THE APPARATUS

The Cleo-Tokamak experiment has been described in several conference reports [1-3]. The toroidal magnetic field strength, $B_\varphi \leq 2$ T at the major radius, R = 0.9 m. The 4 mm thick stainless-steel vacuum vessel has an internal radius of 0.19 m. Two limiters were used in the experiments to be described: one consisting of a 0.18 m radius semi-circle of 10 mm diameter molybdenum rod 0.18 m above the median plane, and the other of a moveable molybdenum block 5 mm thick and 50 mm wide, normally positioned 0.17 m above the median plane. These define an effective limiter radius, a = 0.17 m when the plasma is centered in the vacuum vessel. There is no copper shell and the time constant of the vacuum vessel is only 0.9 ms. Equilibrium is obtained by applying an adjustable vertical field, B_z, external to the vacuum vessel derived from windings in the primary circuit of the iron-cored ohmic heating transformer. The value required for equilibrium is given by Shafranov's formula [4],

$$\frac{B_z}{I_g} = \frac{\mu_o}{4\pi R}\left[\ell n(8R/a) - 3/2 + \ell_i/2 + \beta_\theta\right] \qquad (1)$$

where I_g is the plasma current and $\mu_o \ell_i/4\pi$ is the internal inductance per unit length of the plasma column.

We find experimentally $B_z/I_g = (3.2 \pm 0.2) \times 10^{-7}$ TA^{-1} which corresponds to $\ell_i/2 + \beta_\theta = 0.64 \pm 0.2$. The radial gradient of $B_z\left(= \frac{R}{B_z}\frac{dB_z}{dR}\right) = -0.2 \pm 0.1$. A schematic of the ohmic heating circuit is shown in Fig. 1. The vertical field is supplemented by up to $\pm$ 2 mT from a separate winding driven from a 24 kW power amplifier, whose input is derived from coils, outside the vacuum vessel, measuring the radial position of the plasma current channel.

This system acts as a servo-control [5], maintaining the position constant within $\pm$ 10 mm of the centre of the vacuum vessel for $\geq$ 100 ms and compensating for variations in the vertical field necessary for equilibrium in this position, due, for example, to changes in β_θ. A similar servo-system controls the vertical position of the current channel.

2. DIAGNOSTICS - PLASMA PARAMETERS

2.1. 'STANDARD' DISCHARGE

A typical discharge centred in the vacuum vessel has a plasma current, $I_g \sim$ 60-70 kA; the gap voltage, $U_G \sim 3.5$ V giving a resistive power input $\sim$ 200 kW; the average electron density, $\bar{n}_e \sim 2 \times 10^{19}$ m^{-3}; $\beta_\theta \sim 0.4$ at peak current, increasing as the current decays; the energy confinement time, $\tau_E \sim 3$ ms and the safety factor at the limiter, $q_a \sim 5$. Oscillograms of various parameters are shown in Fig. 3.

The plasma density is measured by a 4 mm μ-wave interferometer, and a 3-channel, 2 mm μ-wave interferometer, whose beams can be traversed radially across a window, gives a density profile. With the usual value of limiter radius, a = 0.17 m, the profile is nearly parabolic after 20 ms. The density is greater than the filling density and the density maximum occurs $\sim$ 20 ms after peak current.

Measurements of H_β light in a narrow pencil scanned across the plasma radius at a point remote from the limiters were made to determine the neutral particle density and particle confinement time. The instrument was calibrated with a standard lamp. The resulting radial distribution of neutral hydrogen density is shown in Fig. 4. The absolute accuracy of these measurements is estimated to be within a factor of two. The particle confinement time cal-

culated from the same data is 10 to 20 ms, although in the absence of measurements near the limiters this result must be somewhat speculative.

A diamagnetic loop is positioned outside the vacuum vessel. Unfortunately it is subject to a certain amount of interference from the horizontal components of the externally applied vertical field. A correction factor of 10 to 20% was determined from measurements on two, otherwise identical discharges with current parallel and anti-parallel to the toroidal field. The corrected value of β_θ is $\sim$ 0.4 at current maximum, increasing as the current decays. Together with the mean density from the interferometer, this gives an average value for $T_\perp = \bar{T}_e + \frac{n_i}{n_e} \bar{T}_i$ of typically 300 eV.

An estimate of the electron temperature has been obtained by incoherent scattering of ruby laser light. The scattered light was spectrally resolved by interference filters and the temperature measured on a shot to shot basis using only two channels. These measurements yield a central electron temperature $T_{eo} = 240 \pm 50$ eV at 20 ms and $T_{eo} = 210 \pm 100$ eV at 50 ms from initiation (current maximum) in a 70 kA discharge. For this case the mean values of conductivity and diamagnetic temperature were $T_\sigma = 85 \pm 3$ eV and $T_\perp = 300 \pm 60$ eV. Higher values of T_σ, up to 105 eV have been measured in some discharges at the same current level, but the corresponding values of T_e were not obtained.

The central ion temperature, T_{io} is shown as a function of time in Fig. 8. It is measured with a neutral particle analyser, which is described in detail in Section 8.1. If the profile of T_i is parabolic $\bar{T}_i = 115 \pm 4$ eV at peak current, which combines with $T_\perp$ to give $\bar{T}_e = 185 \pm 60$ eV. Since $T_{eo} = 210 \pm 100$ eV from

photon scattering, we conclude that the profile of T_e is rather flat. Comparison of $\bar{T}_e$ and T_σ gives $\bar{Z}_{eff} = 5 \pm 2.5$.

The central ion temperature calculated from Artsimovich's formula [6] is 230 eV which compares reasonably well with the measured value of 198 $\pm$ 8 eV. The corresponding value of ion energy confinement time is estimated to be 4 ms.

Three arrays of small coils arranged to pick up B_θ fluctuations are positioned just outside the ceramic break in the vacuum vessel. These measure the amplitude of the M.H.D. oscillations which are usually observed in tokamaks [7]. The angular positions of the coils in each array are chosen to maximise their response to modes with m = 2, 3, 4. In practice, mode discrimination is far from perfect, but the signal from one coil array is usually greater than the other two, and for $q_a \sim 5$ this is usually the set 'tuned' to m = 3. Oscillation frequencies vary in the range 4-15 kHz, being lower when the amplitude is larger. The frequency is measured by a pulse-shaping discriminator followed by a frequency sensitive detector to an accuracy better than 500 Hz.

2.2. 'SCALING' EXPERIMENTS

Two separate experiments were made to determine the smallest value of safety factor at the limiter, q_a which could be obtained without provoking the disruptive instability. In the first the 'radius' of the block limiter was reduced from 0.18 m to 0.10 m at B_φ = 2.0 T, and in the second B_φ was varied between 1.2 T and 2.0 T at a = 0.18 m. In each case disruptive instabilities were observed whenever $q_a \leqslant 4$. During the course of these experiments and others I_g varied between 25 and 80 kA, $\bar{n}_e$ between 0.8×10^{19} and $2.4 \times 10^{19} m^{-3}$ and T_σ between 60 and 115 eV. The following relations have been

found to hold at peak current.

$$n_e = KI_g \tag{2}$$

where $K = (3.3 \pm 0.5) \times 10^{14}\ m^{-3}\ A^{-1}$, almost independent of the filling pressure.

$$U_G = 3.5 \pm 0.5\ V, \tag{3}$$

$$\text{and } \beta_\theta = 0.4 \pm 0.1. \tag{4}$$

The constancy of U_G immediately implies a relation for T_σ of the form

$$T_\sigma^{3/2} = A \frac{I_g}{\pi a^2}. \tag{5}$$

Assuming uniform current density, Spitzer resistivity with $Z = 1$, $\ell n \Lambda = 15$ gives

$$A = (1.27 \pm 0.18) \times 10^{-3} (eV)^{3/2}\ m^2 A^{-1}.$$

If we also assume $\beta_{\theta e}$ is constant at $\frac{2}{3}\beta_\theta$, then we can write, using (2)

$$0.27 = \beta_{\theta e} = \frac{4\pi}{\mu_o} \frac{2\pi a^2\ Ke\ \bar{T}_e}{I_g} \tag{6}$$

$$\text{or} \quad \bar{T}_e = C \frac{I_g}{\pi a^2}, \tag{7}$$

where $C = (2.6 \pm 0.7) \times 10^{-4}\ eV\ m^2 A^{-1}$.

Combining (5) and (7) gives

$$\frac{\bar{T}_e}{T_\sigma} = (2.2 \pm 0.6) \times 10^{-2} \left(\frac{I_g}{\pi a^2} \right)^{\frac{1}{3}}. \tag{8}$$

We conclude that the plasma is dominated by interaction with the vacuum vessel wall: the plasma density increases with increasing current independent of filling pressure, probably due to desorption of material from the wall, and $Z_{eff} = fn\ (\bar{T}_e/T_\sigma)$ increases slowly with current density (or electron temperature). Nevertheless, the plasma behaves pseudoclassically in the sense that $\beta_\theta \sim 0.4$ and is

constant.

3. NEUTRAL INJECTION

The arrangement of the injector and neutral particle detectors is shown in Fig. 2. For all measurements the neutral beam pulse duration is 25 ms, and the source drain current is ~ 5 A. The injector system is discussed in detail in references [8,9,10].

Table 1 summarises estimations of the power trapped in the plasma in terms of that extracted from the ion source. There are losses due to the finite beam divergence (access) and neutralisation efficiency. In addition there are losses because the neutralisation does not reach equilibrium and a serious loss due to re-ionisation of the neutral beam by neutrals in the beam line and subsequent deflexion by the toroidal field of the tokamak. The effect of the latter two losses together was estimated using a calorimeter placed opposite the beam line (Fig. 2.) with the toroidal field switched on and off.

Ionisation of the fast ions in the plasma is efficient, since the dominant mechanism is charge exchange. The estimation of the fraction of the beam on contained orbits was made by numerical computation assuming all ions outside a radius of 0.14 m are lost due to rapid charge exchange with the neutral background shown in Fig. 4 and that the centre of the ion orbits are displaced w.r.t. the magnetic axis by $\Delta = \pm \rho_{i\theta}\, a/R$. $\Delta \sim 50$ mm for Cleo [8].

4. FAST ION SPECTRUM - THEORY

The collisional interaction of the fast ions with the plasma is described by the Fokker-Planck equation [11] for the velocity distribution function f. (The right hand side terms represent respectively: friction, angular scattering, velocity diffusion,

electric acceleration, charge-exchange and the source):

$$\frac{\partial f}{\partial t} = \frac{1}{\tau_s}\left[\frac{1}{v^2}\frac{\partial}{\partial v}\{(v_c^3 + v^3)f\} + \frac{m_i Z_{eff} v_c^3}{2m_b \bar{Z} v^3}\frac{\partial}{\partial \zeta}\{(1-\zeta^2)\frac{\partial f}{\partial \zeta}\}\right.$$

$$\left. + \frac{Dm_e v_e^2}{2m_b v^2}\frac{\partial}{\partial v}\left(v\frac{\partial f}{\partial v}\right)\right] - \frac{Z_b e E^*}{m_b}\left[\frac{(1-\zeta^2)}{v}\frac{\partial f}{\partial \zeta} + \zeta\frac{\partial f}{\partial v}\right]$$

$$- f/\tau_{cx} + S(\zeta, t)\,\delta(v - v_o) \qquad (9)$$

where m_i and m_b are plasma and injected ion masses, $v = (2\epsilon/m_b)^{\frac{1}{2}}$, $v_e = (2kT_e/m_e)^{\frac{1}{2}}$, $v_c = (3\sqrt{\pi}\,\bar{Z}/4)^{\frac{1}{3}}(m_e/m_i)^{\frac{1}{3}} v_e$, $Z_{eff} = \Sigma n_j Z_j^2/n_e$, $\bar{Z} = \Sigma Z_j^2 n_j m_i/n_e m_j$, $\tau_s = 1.25 \times 10^{18} n_e^{-1} A_b Z_b^{-2} [T_e(keV)]^{3/2}$; $E^* = [1 - 1/Z_{eff}]\, U_G/2\pi R_o$, $\zeta = v_{\parallel}/v$, and subscript b refers to injected beam particles. U_G is positive for injection parallel with I_g. The value of $\bar{Z}$ is in the range 0.5 to 1.0 and for typical tokamak conditions [12] $\bar{Z} = 0.9 \sim 1.0$. In deriving the above equation we have assumed that the plasma behaves classically (e.g. classical resistance) and consequently $\bar{T}_e = [0.58\, Z_{eff}/\gamma_E(Z_{eff})]^{\frac{2}{3}} T_\sigma$ where $\gamma_E(Z_{eff})$ is given by Spitzer and Harm [13].

4.1. THE EQUILIBRIUM SOLUTION

The solution of equation (9) in the stationary state is discussed fully in reference [14]. The solution may be written in the form

$$f = \frac{S\tau_s}{(v^3 + v_c^3)1 - \tau_s/3\tau_{cx}}\left[1 + \sum_1^\infty \frac{C_n (v/v_o)^{\rho n(n+1)}}{(v^3 + v_c^3)^{\rho n(n+1)/3}} P_n(\zeta)\right]$$

$$+ O\left(\frac{Z_b e E^* \tau_s}{m_b}\right) \quad \text{for } v < v_o, \text{ and} \qquad (10)$$

$f = A\exp\{-(v - v_o)/v_w\}$ for $v > v_o$, where v_o is the injection velocity with $v_w = DT_e v_o/\{2\epsilon_o(1 + v_c^3/v_o^3 - Z_b eE^* \tau_s \zeta/v_o\}$

$\rho = m_i Z_{eff}/(2m_b \bar{Z})$, and the constants C_n are determined by the injection source rate S in the manner described in Ref [14]. Typical solutions are plotted in Fig. 5. The following points about the solution should be noted.

1) the velocity diffusion term can raise the energy of some of the fast ions above the injection energy. The basic term used in Eq (9) with D = 1 takes account of the diffusion due to collision with electrons.

2) Diffusion can also occur due to collisions between the fast ions and it may be enhanced by instabilities. The factor D in the diffusion term of equation (9) is used so that such additional mechanisms may be taken into account.

3) The width of the high energy tail v_w is enhanced or diminished by the toroidal electric field depending on whether E* is positive (parallel injection) or negative (anti-parallel). Note that E* also depends on Z_{eff}, and is zero for $Z_{eff} = 1$, when the electric acceleration of a fast ion is exactly balanced by the drag from the drifting electrons.

4.2. TIME DEPENDENT SOLUTION

The time dependent solution of Eq (9) is required so that the theoretical and measured slowing down times can be compared. It is calculated numerically [15] and examples of typical time dependent behaviour are given in Fig. 6. For the CLEO parameters the fast ions reach their equilibrium distribution in about $0.8\ \tau_s \sim 8$ ms.

5. FAST ION SPECTRUM - EXPERIMENT

For these measurements approximately 24 kW of H^+ ions are trapped in the discharge at energies ϵ_o = 22.5, 11.25 and 7.5 keV.

The high energy ions are studied, as they slow down, with the high energy neutral particle detector shown in Fig. 2. It consists of a stripping cell (hydrogen), electrostatic deflector and photomultiplier. The energy bandwidth is $\pm$ 3%. Charge exchange ions are collected on a line tangent between 0.90 and 0.95 m major radius, in the median plane, and in the range $0^{o} \rightarrow 20^{o}$ to the main magnetic field. Preliminary results have been reported elsewhere [16].

5.1. QUASI-STATIONARY SPECTRA

The experimental spectra at peak signal level are shown in Fig. 5. The data are corrected to allow for scintillator response ($\sim \epsilon$), the neutralisation rate in the plasma ($< \sigma_{10} v >$) and the stripping cell efficiency. The function $N(\epsilon)/(\Delta\epsilon\, \epsilon^{\frac{1}{2}})$ is plotted, where $N(\epsilon)$ is the corrected count rate at energy ϵ and $\Delta\epsilon$ is the detector bandwidth. The electron density profile is parabolic and the mean density, $\bar{n}_e \sim 1.5 \times 10^{19}$ m^{-3}, the gap voltage, $U_G \sim 3.5$ V and the plasma current, $I_g \sim 60$ kA. The conductivity temperature ($Z = 1$, flat distribution), $T_\sigma \sim 80$ eV. The relative extents of the high energy tails with parallel and anti-parallel injection, together with the accurately known values of ϵ_o, U_G, ζ and $\bar{n}_e$ give a value for $\tau_s\,(1 - 1/Z_{eff})$, which is a function of T_e and Z_{eff}. Combining with the accurately known T_σ, which is also a function of T_e and Z_{eff}, we find $T_e = 280$ eV ($\tau_s = 10$ ms) and $Z_{eff} = 6.7$, which are consistent with the values obtained from other measurements (Section 2).

The spectra calculated from the theory of Section 4 for the above plasma parameters with a neutral hydrogen density $n_H = 10^{15}$ m^{-3} are also shown in Fig. 5. Excellent agreement with the experimental

results is apparent. The theoretical spectra are not very sensitive to neutral densities less than 1.5×10^{15} m^{-3}, which is valid for the central region of the plasma where the bulk of the fast ions are confined (Fig. 4.) We shall see (Section 8) that the neutral density increases by a factor of two when the neutral beam is switched on, but we believe this is a local effect which does not significantly affect the average neutral density encountered by the fast ions.

The one point of significant disagreement is in the extent of the high energy tails, and to fit the data we had to use $D = 4$, that is four times the diffusion level expected from collisions with electrons. The calculated hot ion density lies in the range 10^{17} to 10^{18} m^{-3}. At the higher density the increased diffusion can be explained entirely by collisions between the hot ions themselves. However, since their density is not accurately known we can not rule out the possibility of velocity diffusion due to instabilities, either naturally present in the plasma or induced by the beam.

5.2. TIME DEPENDENT SIGNALS

The time dependent signals in the region of 22.5 keV are compared with the theoretical model of Section 4 in Fig. 6, using the parameters given above. The good agreement of theory and experiment again indicates that the slowing down of the ions is classical. In addition the high diffusion rate is also observed in the temporal behaviour. The charge exchange signals do not reach a steady value during the period of injection but decay following a peak at $\sim$ 6 ms, even though the beam is maintained for 25 ms. We suspect this occurs because of changes in the neutral density in the region of the beam. Initially, this may rise due to gas devolved from the torus wall by

the beam itself, but later on it may decay again because the wall becomes conditioned by the beam. For this reason, in comparing with the theory, the ratio between signals at two different energies is plotted so that changes in neutral density are compensated.

5.3. TOTAL CONFINED ENERGY OF FAST IONS

The mean value of Γ, the ratio of the total energy in the fast ions to that in the plasma, calculated from the theoretical spectra shown in Fig. 5, is 0.14.

6. EXPECTED PLASMA HEATING - CLASSICAL ENERGY TRANSFER

In this section we extend the treatment given in Reference [8]. The power, injected into the plasma by the neutral beam will disturb the balance between the ohmic power input and the power lost by thermal conduction, diffusion, radiation, etc. In general the plasma temperature will rise, but we should not ignore other effects of the neutral beam in changing the plasma density or the current, and thus indirectly affecting the thermal equilibrium.

For the small (up to 20%) changes in plasma parameters considered here, we consider only first order perturbations in the balance of heating and losses. It is then only necessary to know how the heating and loss rates scale with the plasma parameters, $\bar{n}_e$, $\bar{T}_e$, $\bar{T}_i$, I_g in order to calculate the change in the energy balance. We assume that the plasma profiles are unaffected by injection.

A further simplification can be made by applying Artsimovich's results [6] on the energy balance in Tokamaks, which show that the electron and ion components can be considered separately. This occurs because most of the ohmic heating power delivered to the electrons is lost by non-classical electron thermal conduction and not by equipartition to the ion component.

Assuming the plasma resistance only depends on T_e and that the energy loss rate scales pseudoclassically, as suggested by the results of section 2.2, we can write

$$H_e \sim I_g^{\,2}\, T_e^{\,\alpha}$$
$$L_e \sim n_e^{\,2}\, I_g^{\,-2}\, T_e^{\,\alpha+2} \qquad (11)$$

where H_e and L_e are the heating and loss rates respectively, for ohmic heating alone. Adding power P_e by neutral injection then produces changes Δn_e, ΔT_e, ΔI_g which are related by

$$\frac{P_e}{H_e} = 2\,\frac{\Delta n_e}{n_e} - 4\,\frac{\Delta I_g}{I_g} + 2\,\frac{\Delta T_e}{T_e}$$

or

$$\frac{\Delta T_e}{T_e} = \tfrac{1}{2}\left[\frac{P}{H_e} - 2\,\frac{\Delta n_e}{n_e} + 4\,\frac{\Delta I_g}{I_g}\right]. \qquad (12)$$

For the ion component, we assume energy gained by classical equipartition and lost by neoclassical thermal conduction in the intermediate regime. These assumptions lead to a scaling law for ion energy with strong experimental support [6] although the loss mechanism may not always be solely due to neoclassical processes. We take,

$$H_i \sim n_e^{\,2}\, T_i^{\,-\frac{1}{2}}$$
$$L_i \sim T_i^{\,5/2}\, n_e\, I_g^{\,-1}, \qquad (13)$$

which leads to

$$\frac{\Delta T_i}{T_i} = \tfrac{1}{3}\left[\frac{P_i}{H_i} + \frac{\Delta n_e}{n_e} + \frac{\Delta I_g}{I_g}\right]. \qquad (14)$$

For the undisturbed plasma we take a total ohmic power input of 200 kW of which the ions receive 47 kW via equipartition, $\bar{n}_e = 2 \times 10^{13}$ cm^{-3}, $\bar{T}_i = 100$ eV, $\bar{T}_e = 200$ eV. After injection we

observed $\Delta n_e/n_e \sim 0.05 \pm 0.02$, $\Delta I_g/I_g < 0.005$. We calculate the power input to the electrons from the injected beam (5 A drain current) using classical coefficients and the results of Section 4.1. to be 11 kW, and the power input directly to the ions 10 kW.[1] Substituting these results in equation (12) gives $\Delta T_e/T_e = - 0.02 \pm 0.02$, ie practically no change. $\Delta T_i/T_i$ calculated from equation (14) is 0.09 ± 0.01.

If we assume the ion component accounts for about one third of the plasma energy the expected increase in β_θ due to changes in plasma density and temperature, $\Delta\beta_{\theta p}$ is 0.026 ± 0.011. This is compared with experiment in the next Section. (See equation 20).

7. MACROSCOPIC EFFECTS OF NEUTRAL INJECTION

At the usual level of injected power, with ~ 24 kW of injected H^+ ions on confined orbits, there is very little disturbance to the main parameters of the plasma. Fig. 7 shows the effect of injection parallel to the plasma current on various measurements. The data were recorded by a data acquisition system [17] with an accuracy of ~ 0.4%. Six pairs of shots with and without injection are compared, by differencing the data at time intervals of 5 ms, and then averaging.

7.1. ELECTRON DENSITY

The change in electron density increases almost linearly from the time of injection with a slope which is equivalent to adding electrons at the rate of 4.5 A. This compares with a neutral hydrogen beam current entering the torus of 2.6 A (equiv.) calculated from the

---

[1] The sum is not necessarily equal to the power in the injected beam. The fast ions also lose energy by charge exchange and gain energy from the toroidal electric field.

figures given in Table I and the measured source drain. Thus, between 1 and 2 electrons are added for each hydrogen beam atom injected.

7.2. RESISTANCE

No significant effect on the gap voltage, U_G or plasma current I_g can be detected. The change in U_G, $\Delta U_G < 200$ mV ($\sim 6\%$) and $\Delta I_g < 300$ A ($\sim 0.4\%$). These results imply that the conductivity temperature changes by no more than 4%. Similar results are obtained on the A.T.C. tokamak [18]. The fast ion velocity distribution is calculated numerically by the method discussed in Section 4. From this we can estimate the circulating current of fast ions, $I_b = 1$ kA. Following the method of Ohkawa [19], we calculate the corresponding change in resistivity of the plasma to be given by

$$\eta = \eta_o \left[1 + \frac{I_b (Z_b / Z_{eff} - 1)}{I_g} \right] \qquad (15)$$

where η_o is the resistivity in the absence of beam and Z_b is the fast ion charge. For $I_b = 1$ kA, $I_g = 70$ kA, $Z_b = 1$, $Z_{eff} = 5.5$ a - 1.2% change in plasma resistance should be observed, unfortunately this is beyond our detection limit of 6%. We do not expect to see any change in the plasma current $> 0.25\%$ because the resistance in the primary circuit of the O.H. transformer (Fig. 1) is larger than the plasma resistance (reflected into the primary) by a factor of 5 x.

7.3. HOOP FORCE AND PLASMA PRESSURE

The output of the power amplifier controlling the plasma position is a sensitive monitor of the outward force on the plasma column. During injection this force should be increased by any increase in the plasma pressure, and also by the (mainly centrifugal)

force of the confined high energy ions from the beam.

The total outward force on the plasma column due to all the confined particles can be written

$$f_{out} = \frac{1}{R} \sum_j m_j \, (v_{\perp j}^2/2 + v_{\parallel j}^2) \qquad (16)$$

where m_j, $v_{\perp j}$ and $v_{\parallel j}$ are respectively the mass and the components of velocity perpendicular and parallel to the magnetic field of the j^{th} particle. For an isotropic velocity distribution equation (16) corresponds with the β_θ term in equation (1). However, the plasma diamagnetism is proportional to the flux displaced by all the particles in the plasma, that is to $\sum_j m_j v_{\perp j}^2$, and this is the quantity measured by the diamagnetic loop. Because the velocity distribution of the confined high energy ions is not isotropic we must rewrite equation (1) as:

$$\frac{B_{zs} + B_{zp}}{I_g} = \frac{\mu_o}{4\pi R}\left[\ell n\left(\frac{8R}{a}\right) - \frac{3}{2} + \frac{\ell_i}{2} + \beta_{\theta p} + A\, \beta_{\theta b} \right] . \qquad (17)$$

Here, B_{zs} is the part of the vertical field produced by the control amplifier and B_{zp} the part produced by the primary circuit; $\beta_{\theta p}$ is the diamagnetism of the background plasma (isotropic velocity distribution), $\beta_{\theta b}$ is the diamagnetism of the fast ions from the injected beam and

$$A = \sum_b (v_{\perp b}^2/2 + v_{\parallel b}^2)/\sum_b v_{\perp b}^2 \qquad (18)$$

where the sums are over the beam ions only.

Upon injection B_{zp}/I_g does not change, since the primary and plasma circuits are closely coupled by the iron-cored transformer. We also assume R, a and ℓ_i are constant. The latter is very reasonable, since ΔI_g is very small and the plasma will tend to preserve the current distribution. Equation (17) then gives

$$\frac{\Delta B_{zs}}{I_g} = \frac{\mu_o}{4\pi R}\left[\Delta\beta_{\theta p} + A\,\Delta\beta_{\theta b}\right] \qquad (19)$$

where we have neglected $B_{zs}\Delta I_g/I_g$ compared with ΔB_{zs}.

Fig. 7(e) shows ΔB_{zs} to be easily measureable: it is $(2.5 \pm 0.5) \times 10^{-4}$ T. Putting $I_g = 7 \times 10^4$ A, R = 0.9 m in (19) then gives

$$\Delta\beta_{\theta p} + A\,\Delta\beta_{\theta b} = 0.032 \pm 0.006 \,. \qquad (20)$$

The diamagnetic loop also indicates an increase as shown in Fig. 7(f), although in this case the sensitivity of the measurement is worsened by non-reproducibility in the signal during the first 20 ms of the discharge, and by drift in the following integrator. The diamagnetic loop gives

$$\Delta\beta_{\theta p} + \Delta\beta_{\theta b} = 0.05 \pm 0.01 \quad \text{(estimated error)}. \qquad (21)$$

We can estimate $\Delta\beta_{\theta b}$ and A from the velocity distribution of the fast ions, calculated in Section 4. This gives $\Delta\beta_{\theta b} = 0.034$, A = 1.9. $\Delta\beta_{\theta p}$ from the theory of Section 6 is 0.026 ± 0.011. We conclude that we can explain the observed increase in β_θ as measured by the diamagnetic loop, but the increase in the outward force, although just consistent with the measured $\Delta\beta_\theta$ for an isotropic velocity distribution, is a factor 2.9 smaller than expected.

7.4. AZIMUTHAL VELOCITY

The momentum of a tangentially injected beam which is trapped in the plasma may be expected to change the major azimuthal velocity of the plasma, and of waves within it. We have looked for changes in the frequency of the M.H.D. instabilities during injection, but have observed no change greater than 1 kHz. The corresponding change in the azimuthal velocity of the plasma is less than 6×10^3 ms^{-1} (2% of the sound speed), unless accompanied by a

compensating change in the rotation speed about the minor axis. This velocity refers to the radial position in the plasma where the instability is localised, which we do not know precisely. Work on the ST tokamak using the Thallium beam diagnostic showed an instability of similar type localised near the radius where $q_r = m$ [20]. Assuming a parabolic current density profile with $q_a = 5.5$ and $m = 3$, gives a radial position for the instability of 70 mm. Plasma velocities inside this radius could be higher. However, if we assume the above velocity change is a mean value we can calculate a momentum confinement time, τ_m: the ratio between the change in ϕ momentum and the rate of injection of momentum from the beam. τ_m is less than 3 ms, which is much smaller than the particle confinement time estimated from absolute measurements of H_β light of 10-20 ms. This low value could be due to

1) Compensating changes in velocity about the minor axis.

2) Strong shear in v_ϕ, with much higher velocities in the centre of the plasma, although in this case we might expect to see an increase in the equilibrium vertical field, which is not observed (Section 7.3.)

3) Damping of the toroidal velocity by mechanisms such as those suggested by Cônnor and Cordey [21].

7.5. HIGH POWER INJECTION

At higher injected power levels, up to 80 kW, with the beam parallel to the plasma current the plasma density rises non-linearly with beam current. We believe this is caused by part of the beam striking the inner wall of the torus and devolving cold gas from it. The effect is variable and depends to some extent on the

condition of the wall. In this case also, an increase in β_θ and a corresponding increase in the control amplifier current are seen. No change is observed in the frequency of the M.H.D. oscillations.

8. MEASURED BACKGROUND ION DISTRIBUTION

8.1. NEUTRAL PARTICLE ANALYSER

Neutral particles with energies in the range 200 eV to 5.4 keV are analysed with a multi-channel electrostatic analyser with funnel channelled multipliers (Mullard 419 B6 channeltrons) as detectors. The system is similar to that used by Barnett and Ray [22]. The channeltrons are biased to 3 kV so that their counting rate efficiency is independent of the particle energy [23]. Hydrogen is used in the stripping cell.

The analyser is calibrated using a duoplasmatron ion source with a magnetic mass separator. An additional gas chamber is used to neutralise the ion beam, and the neutralised beam is measured by a Faraday cup with a known secondary emission coefficient as a function of energy [22].

The position of the analyser is shown in Fig. 2. It does not have a magnetic screen, but the stray fields measured at the analyser are $B_\varphi \leqslant 0.15$ mT, $B_R \leqslant 0.15$, $B_z \leqslant 1$ mT. The magnitude and geometry are such that they could not give a serious distortion of the measured distribution function, but at most a 2% displacement along the energy axis.

8.2. LOW ENERGY ION SPECTRUM

The ion distribution function, deduced from measurements of the neutral flux versus energy in the case without injection, is shown in Fig. 9. We obtain the usual two component spectrum [6] in

which the part above 500 eV is linear and is taken to represent the central ion temperature. The absolute value of the ion temperature can be evaluated within an experimental accuracy + 20%, - 15%. This limitation is largely due to the complicated calibration. However, the accuracy of the relative measurement is usually better than 5 to 6% as discussed below.

The variation of ion temperature during one 70 kA discharge is shown in Fig. 8. The temperature of the ions is almost constant at 190 eV from 30 ms onwards. This result made it possible for us to measure the change of ion temperature when neutral injection was switched on during a pulse.

Since the neutral particle count rate at 1.8 keV is a sensitive function of n_o and T_i, it is worth noting that the measured value is within a factor of three of that expected for a plasma with T_i = 190 eV, $n_e = 2 \times 10^{19}$ m^{-3}, $n_o \sim 10^{15}$ m^{-3}.

8.3. ION SPECTRUM WITH INJECTION

Most of our results were taken with a source drain current of 5 A. The beam is usually injected 40 ms after the start of the discharge. The ion distribution function with neutral injection is shown in Fig.9 for two different times 45 ms and 60 ms after the start of the discharge and can be compared with the case of no injection. All the data are averaged over several shots. The three distribution functions are normalized at an energy ϵ = 500 eV.

There is a large deformation of the ion distribution function with injection. It is still possible to fit a straight line to the distribution function in the energy interval 600-1800 eV, but there is now a relatively high level of particles with energies in the range 1.8 to 5.4 keV. Such a tail to the distribution

function persists during the decay of the injector pulse but at about half the level (Fig. 9 curve 3) and has disappeared by 75 ms. The theory of Section 4 predicts the presence of such a tail because of the scattering of slowed down injected particles into the perpendicular direction. This flux should exceed the thermal flux for energies $\epsilon > 1.4$ keV. Fig. 10 shows a comparison between the measured and theoretically calculated spectra in this energy range. The correspondence is good for $Z_{eff} = 5 \pm 1.5$ which agrees with the estimates of Sections 2 and 5.

The absolute value of the ion temperature estimated from the slope of the distribution function in the region 0.6 to 1.8 keV is 225 ± 9 eV with injection, compared with 198 ± 8 eV without injection, giving $\Delta T_i/T_i = 14\% \pm 6\%$. This compares with the $9\% \pm 1\%$ calculated in Section 6.

It should be noted that the absolute value of the neutral particle flux increases by approximately a factor of two even at $\epsilon \sim 500$ eV when the injection is switched on. This result is not difficult to explain in view of the fact that some of the injected neutrals and ions can bombard the torus wall just near the neutral particle detector and hence release thermal neutrals into the plasma.

9. CONCLUSIONS

The injection of a beam of high energy neutrals into a tokamak plasma can be used to raise the temperature of the plasma ions. The observed heating of the background ions is in good agreement with that expected on the basis of classical collisional energy transfer.

At the present level of injected power (a small fraction of the total power input to the plasma) no serious disturbance of the

plasma equilibrium is observed. We observe a small increase in the transverse plasma pressure consistent with the increases in plasma density and ion temperature.

We did not detect any change in the azimuthal velocity of the plasma, nor did we observe the change in the equilibrium vertical field which should result from the centrifugal force of the confined high energy ions.

The fast ions appear to transfer their energy to the plasma by classical processes. The time dependent and quasi-stationary form of the fast ion spectrum at energies below the injection energy show excellent agreement with numerical calculations based on the Fokker-Planck equation. However, the velocity diffusion of the fast ions appears to be a factor of four larger than that expected. Self-collisions or instabilities are the most likely explanations of this observation. The observed slow decay of the fast ion spectra during the injection pulse is not yet satisfactorily explained.

ACKNOWLEDGEMENTS

We are grateful for the efforts of the Cleo-Tokamak operating team and of the Heating and Injection Group in the course of this work. Drs R.J. Bickerton and A. Gibson initiated the program which produced the results presented here, and we should like to acknowledge their continued support and interest.

REFERENCES

[1] GIBSON, A., et al, Paper B16-I Third Int. Symp. on Toroidal Plasma Confinement, Garching (1973).

[2] PAUL, J.W.M., et al, Paper 1.1.2 Sixth European Conf. on Controlled Fusion and Plasma Physics, Moscow (1973).

[3] HUGILL, J. et al, Paper 1.7.2 Sixth European Conf. on Controlled Fusion and Plasma Physics, Moscow (1973).

[4] SHAFRANOV, V.D., Reviews of Plasma Physics 2, Consultants Bureau, New York (1966) p.103.

[5] HUGILL, J., GIBSON, A., Nuclear Fusion 14 (1974)

[6] ARTSIMOVICH, L.A., Nuclear Fusion 12 (1972) 242 (Section 12).

[7] MIRNOV, S.V., SEMENOV, I.B., Sov. Atomic Energy 30 (1971) 22.

[8] ALDCROFT, D., BURCHAM, J., COLE, H.C., COWLIN, M., SHEFFIELD, J., Nuclear Fusion 13 (1973) 393.

[9] SHEFFIELD, J., et al, Paper 1.3.1. Sixth European Conf. on Controlled Fusion and Plasma Physics, Moscow, (1973).

[10] COWLIN, M.L., et al, Paper 25 Eighth Symposium on Fusion Technology, Jutphaas, (1974).

[11] ROSENBLUTH, M.N., MACDONALD, W.M., JUDD, D.L., Phys. Rev. 107 (1957) 1.

[12] HINNOV, E., Princeton Plasma Physics Lab Report MATT-1022 (1974).

[13] SPITZER, L., HARM, R., Phys. Rev. 89 (1953) 977.

[14] CORDEY, J.G., CORE, W.G.F., Physics of Fluids 17 (1974) 1626.

[15] CORDEY, J.G., CORE, W.G.F., Private communication.

[16] SHEFFIELD, J., CORDEY, J.G., et al, Supplement to Paper 1.3.1. Sixth European Conf. on Controlled Fusion and Plasma Physics, Moscow (1973).

[17] MURPHY, E.G., FULLARD, K., STEED, C.A., Proc. 7th Symp. on Fusion Technology, Grenoble (1972) 77.

[18] BOL, K., CECCHI, J.L., DAUGHNEY, C.C., ELLIS, R.A. Jr., EUBANK, H.P., FURTH, H.P., GOLDSTON, R.J., HSUAN, H., JACOBSEN, R.A., MAZZUCATO, E., SMITH, R.R., STIX, T.H., Phys. Rev. Lett. 32 (1974) 661.

[19] OHKAWA, T., Nuclear Fusion 10 (1970) 185.

[20] JOBES, F.C., HOSEA, J.C., Paper B14, 3rd Int. Symp. on Toroidal Plasma Confinement, Garching (1973).

[21] CONNOR, J.W., CORDEY, J.G., Nuclear Fusion 14 (1974) 185.

[22] BARNETT, C.F., RAY, J.A., Nuclear Fusion 12 (1972) 65.

[23] FOX, J.N., FITZWILSON, R.L., THOMAS, E.W., Journ. of Sci. Instr. 3 (1970) 36.

TABLE 1. CALCULATED BEAM POWER TRAPPED IN THE TOKAMAK PLASMA

	HYDROGEN		
	H^+	H_2^+	H_3^+
1. Fractions of different ions extracted from the source	0.65	0.20	0.15
2. Equilibrium neutralisation fraction on a thick target (calculated)	0.78	0.88	0.88
3. Neutral flux per amp of source drain (equivalent amps)	0.51	0.35	0.40
4. Neutral particle energy (keV)	22.5	11.2	7.5
5. Fraction of beam reionised by gas in the beam line. (Experimental measurement - takes account of incomplete neutralisation on the target)	(Experimental) 0.2	0.2	0.2
6. Fraction of beam in the access aperture: 110 mm diameter at 1.35 m, estimated from beam divergence	0.6	0.6	0.6
7. Fraction of beam reaching the plasma which is ionised	>0.95	>0.95	>0.95
8. Fraction of ionised beam on contained orbits (computer calc.)	0.59	0.72	0.75
9. Total beam current trapped per amp of source drain (amp equiv) (Usual source drain 5 A)	0.14 (0.7A	0.11 0.55A	0.14 0.7A)
10. Total trapped power per kW of source drain (kW)	0.14	0.055	0.047
		0.24	

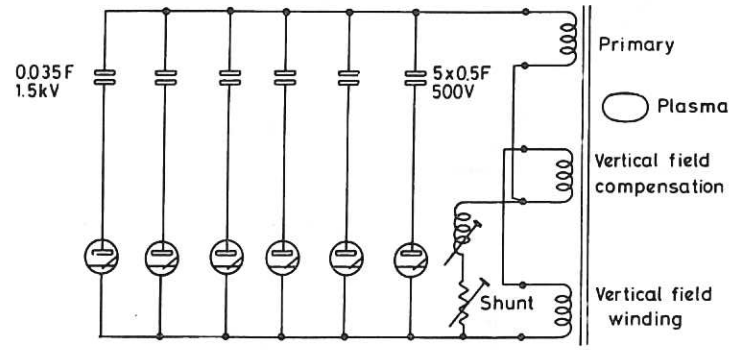

Fig.1 Schematic of the ohmic heating circuit.

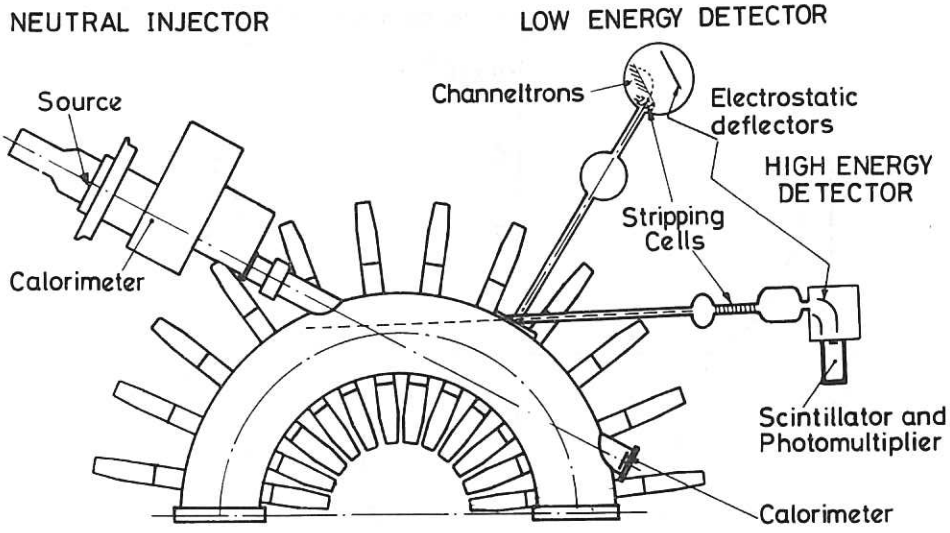

Fig.2 Plan view showing the relative positions of the neutral injector and high and low-energy neutral particle detectors.

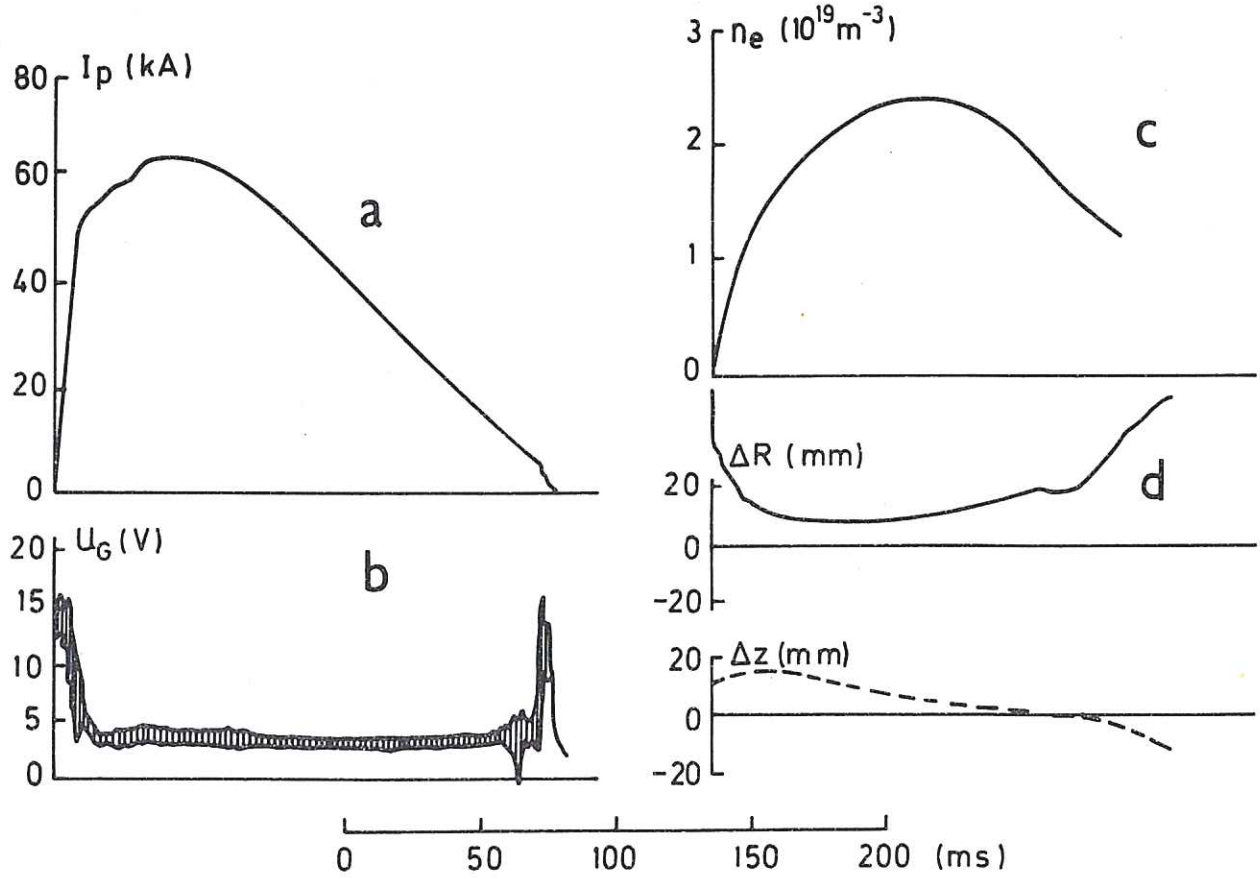

Fig.3 Plasma parameters during a typical discharge (a) Plasma current, (b) Gap voltage, (c) Electron density from 4 mm interferometer and (d) Discharge position _____ radial _ _ _ _ _ _ vertical.

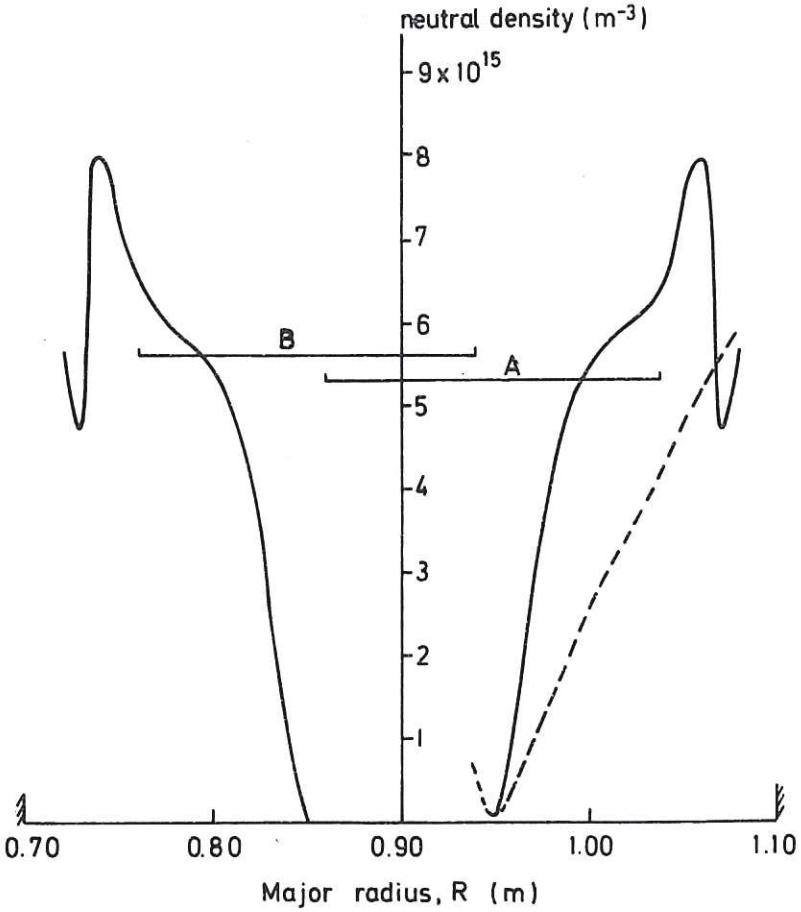

Fig.4 Solid line – radial profile of neutral density calculated from H_β light. A, B – assumed extent of high energy ion orbits for parallel and anti-parallel injection respectively. Dotted line – neutral density averaged over ion orbits for parallel injection.

CLM P407

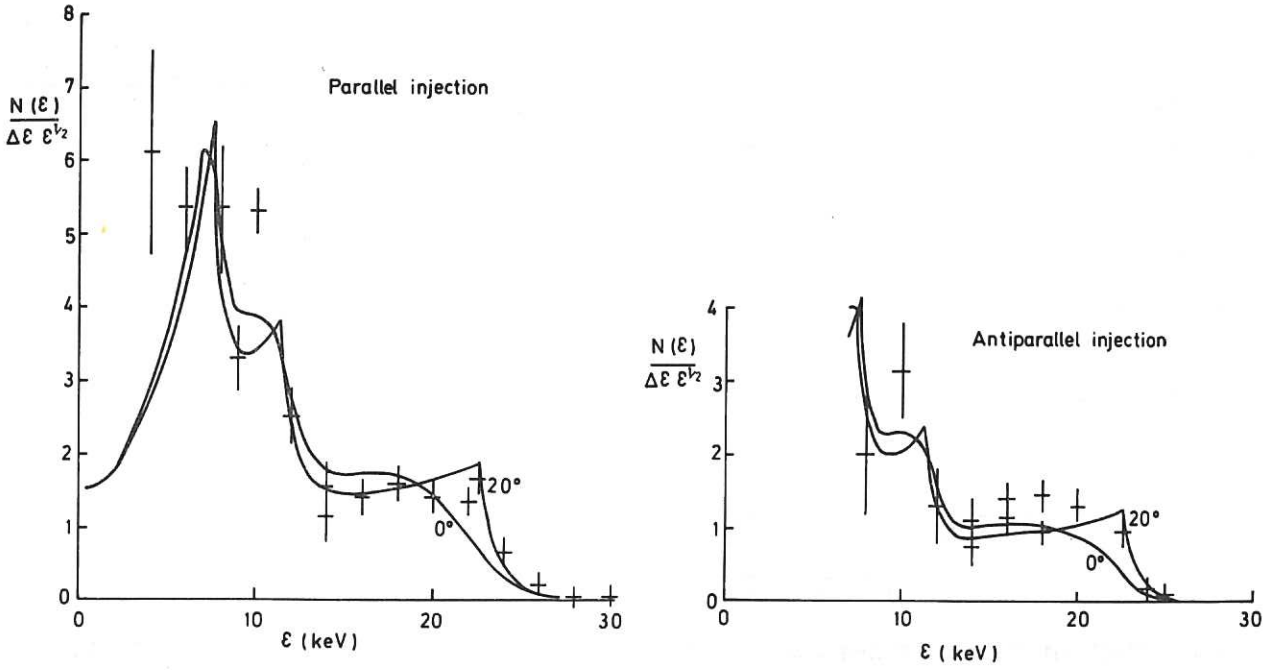

Fig.5 A comparison of the energy spectra of high energy ions measured by the high energy neutral particle detector approximately 6 ms after the injection of a hydrogen beam, with the spectra calculated theoretically in Section 4, for injection parallel and anti-parallel to the plasma current. $\bar{T}_e$ = 280 eV, Z_{eff} = 6.7, D = 4, $\bar{n}_H = 1.0 \times 10^{15}$ m^{-3}.

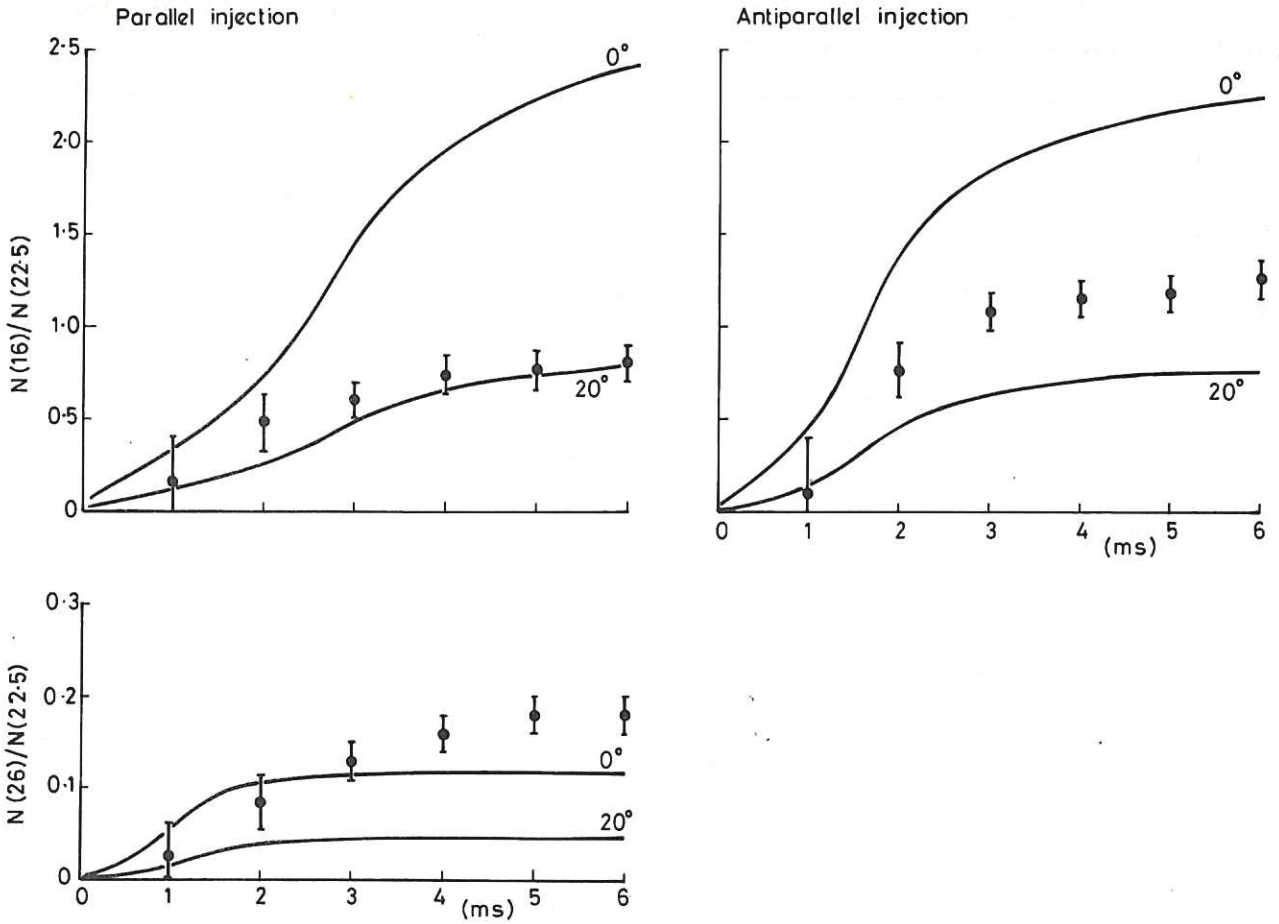

Fig.6 Time development of the high energy ion population above and below the injected energy (22.5 keV) compared with the theoretical model of Section 4. The signals are normalised to that at the injected energy, so as to compensate the variation with time of the neutral density and beam current. Plasma parameters as for Fig.5.

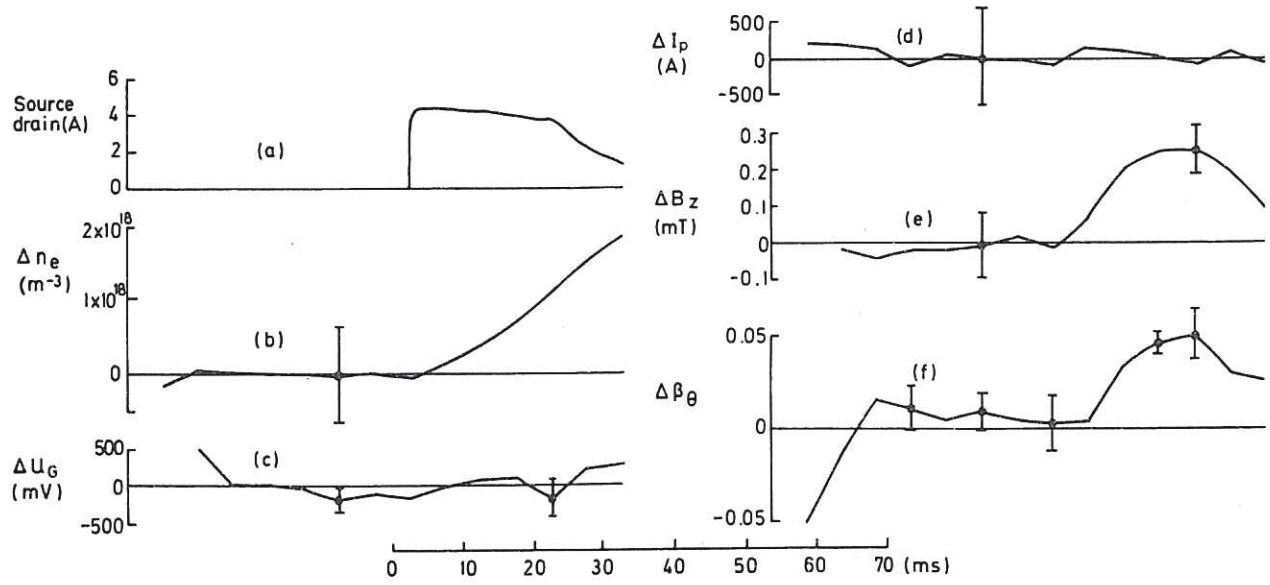

Fig.7 Effects of the neutral beam on the plasma parameters. (a) Source drain current, (b) Electron density measured by 4 mm μ-wave zebra-stripe interferometer, (c) Gap voltage, (d) Plasma current, (e) Field applied by servo-system controlling the plasma position, and (f) Plasma beta calculated from diamagnetic loop signal.

The data are averages of six pairs of shots with and without injection. The indicated error bars are standard deviations, including the effect of shot to shot variation in signal magnitude, but the reproducibility of the shape of most of the signals is better, as indicated by the smoothness of the averaged data before injection.

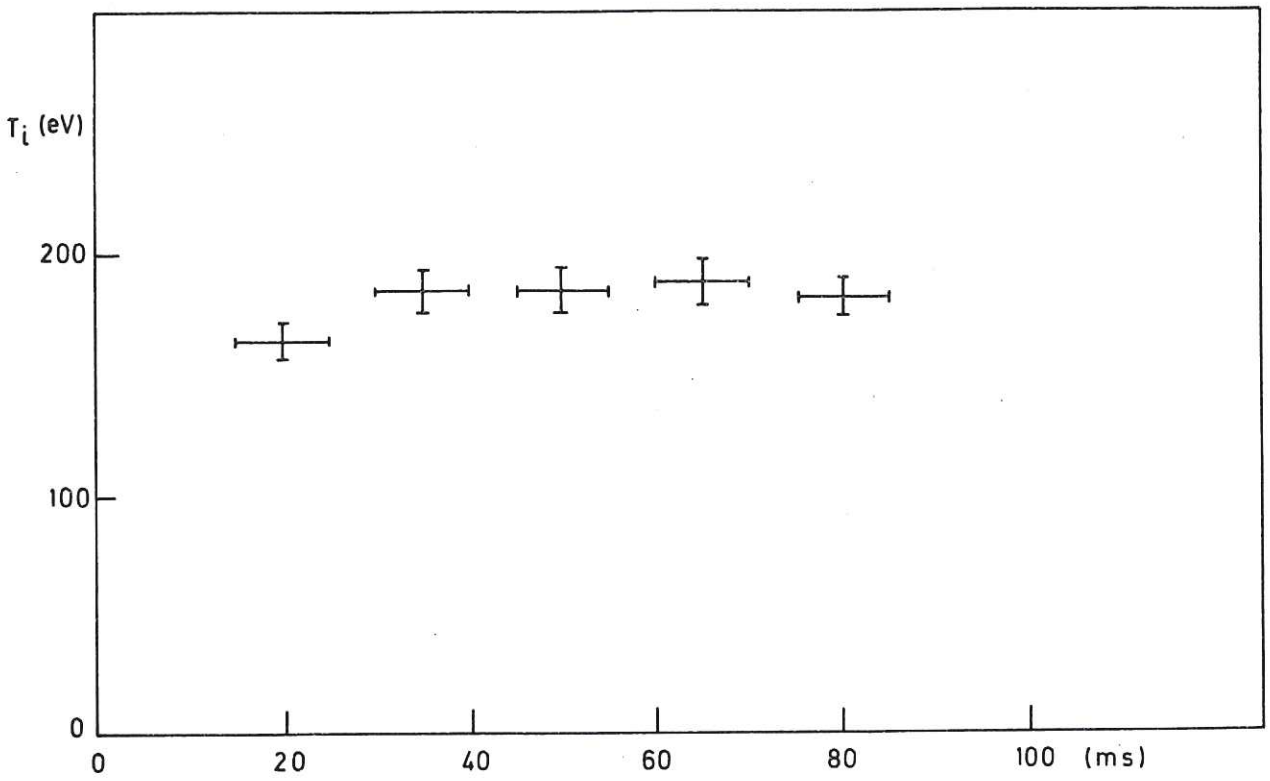

Fig.8 Development of T_i in time as measured by the low energy neutral particle detector. Artsimovich's scaling [6]gives T_i = 230 eV.

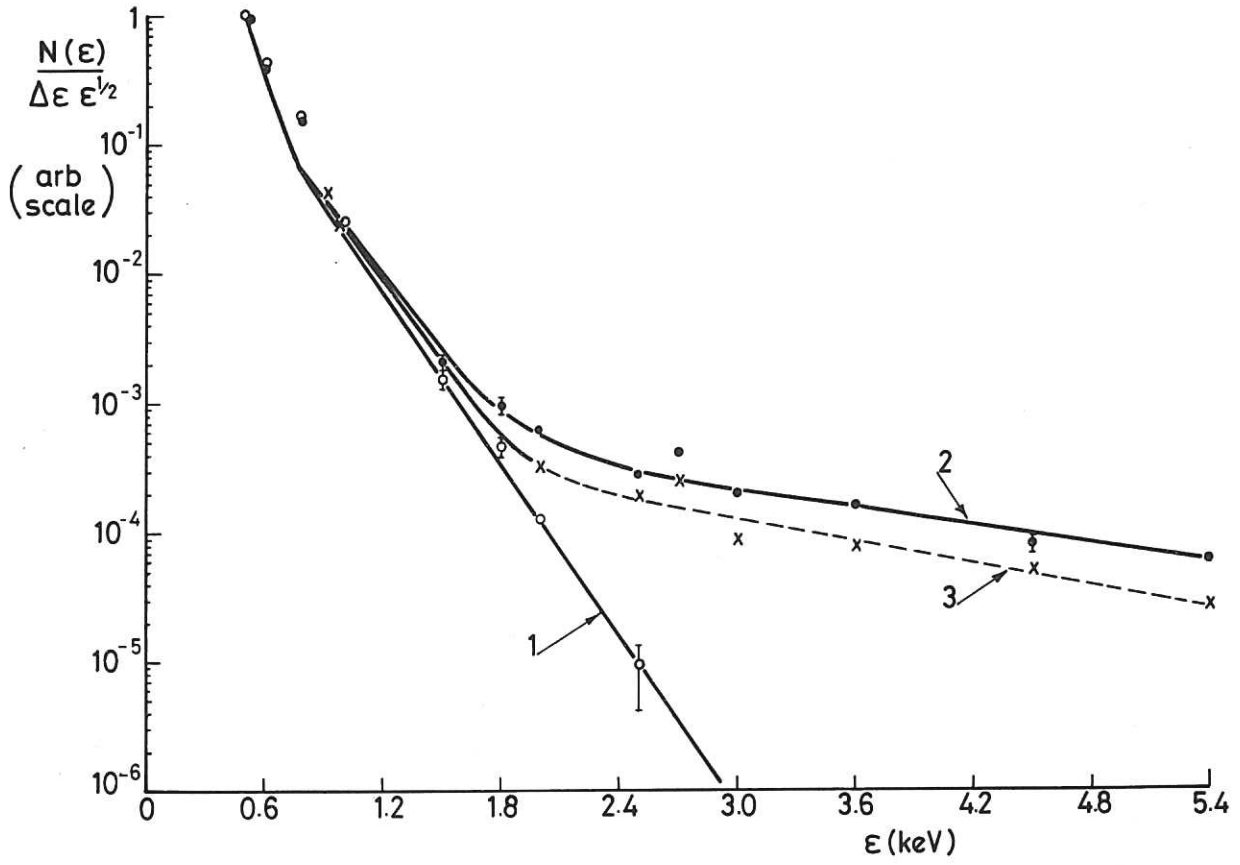

Fig.9 Spectrum of charge exchange neutrals up to 5 keV as measured by the low energy neutral particle detector

Curve 1 No injection
Curve 2 5 ms after injection
Curve 3 20 ms after injection, during the decay of the injector pulse.

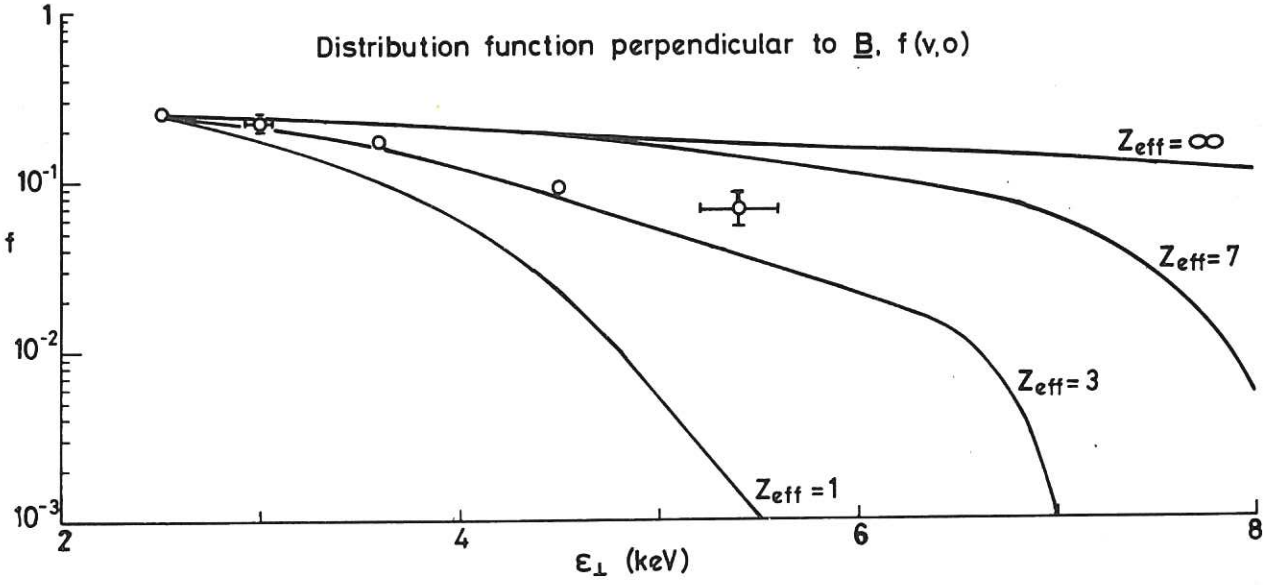

Fig.10 Comparison of the measured tail in the perpendicular spectrum of low energy ions with computed spectra for the slowed and scattered injected ions for various values of Z_{eff}. Experimental and theoretical curves are normalised at 2.5 keV.